Geophysical Research Letters

RESEARCH LETTER
10.1029/2018GL078895

Key Points:
- New parameterization to explain unexpected observations of N_2O in the mesosphere-lower thermosphere (MLT) based on secondary electrons
- Model simulations reproduce spatial and seasonal N_2O variations from recent satellite observations providing quantitative support
- Photoelectrons are principal source for MLT N_2O production outside of high latitudes where energetic electron precipitation dominates

Supporting Information:
- Supporting Information S1

Correspondence to:
C. W. Kelly and M. P. Chipperfield,
eecwk@leeds.ac.uk;
m.chipperfield@leeds.ac.uk

Citation:
Kelly, C. W., Chipperfield, M. P., Plane, J. M. C., Feng, W., Sheese, P. E., Walker, K. A., & Boone, C. D. (2018). An explanation for the nitrous oxide layer observed in the mesopause region. *Geophysical Research Letters*, *45*, 7818–7827. https://doi.org/10.1029/2018GL078895

Received 23 MAY 2018
Accepted 16 JUL 2018
Accepted article online 24 JUL 2018
Published online 8 AUG 2018

An Explanation for the Nitrous Oxide Layer Observed in the Mesopause Region

C. W. Kelly[1], M. P. Chipperfield[1,2], J. M. C. Plane[3], W. Feng[1,3,4], P. E. Sheese[5], K. A. Walker[5], and C. D. Boone[6]

[1]School of Earth and Environment, University of Leeds, Leeds, UK, [2]National Centre for Earth Observation, University of Leeds, Leeds, UK, [3]School of Chemistry, University of Leeds, Leeds, UK, [4]National Centre for Atmospheric Science, University of Leeds, Leeds, UK, [5]Department of Physics, University of Toronto, Toronto, Ontario, Canada, [6]Department of Chemistry, University of Waterloo, Waterloo, Ontario, Canada

Abstract Recent satellite measurements of a layer of enhanced nitrous oxide (N_2O) in the mesosphere-lower thermosphere (MLT) from the Atmospheric Chemistry Experiment-Fourier Transform Spectrometer have suggested an unexpected, minor high-altitude production source. Here we report the development of a mechanism and the first model simulations, which can explain the formation of this MLT N_2O layer. N_2O production occurs primarily via a reaction route involving the excitation of N_2 from secondary electrons. Simulations using the Whole Atmosphere Community Climate Model, with external forcing from the Global Airglow model, quantitatively reproduce the observed vertical, latitudinal, and seasonal N_2O variations. Sensitivity results indicate that photoelectrons are far more important than previously predicted, causing approximately two thirds of global N_2O production in the MLT. Energetic electron precipitation over high latitudes provides the remaining contribution. Solar cycle analysis reveals N_2O enhancements of up to ×2 at solar maximum compared to solar minimum.

Plain Language Summary Nitrous oxide (N_2O) is an important gas in the Earth's atmosphere as it is a greenhouse gas and leads to the production of other nitrogen species that can deplete the ozone layer. It was previously assumed to only be produced at the Earth's surface, primarily through bacterial processes in soil. However, a minor upper atmospheric source has recently been identified from satellite observations. The key aim of this study is to find a plausible mechanism for the source of the observed N_2O based on current knowledge. We compare chemistry-climate model simulations including likely chemical reactions and mechanisms to the satellite measurements. The model matches the observed spatial and seasonal N_2O variations. We also compare simulations with some of the N_2O production processes switched off. These results indicate that N_2O is constantly made through a chemical process involving the arrival of electrons trapped by the Earth's magnetic field near the poles, and light from the Sun at all latitudes. It should be emphasized that the concentration of N_2O in the upper atmosphere is extremely small compared to the concentration of N_2O in the lower atmosphere.

1. Introduction

The major source of nitrous oxide (N_2O) present in the Earth's atmosphere is from surface emissions. The primary production mechanism for this involves nitrification and denitrification bacterial processes in soil (Brasseur & Solomon, 2005). N_2O is then transported into and through the stratosphere via the Brewer-Dobson circulation (Brewer, 1949; Dobson, 1956). It is well known that N_2O is a precursor to stratospheric NO_x (=NO + NO_2), which depletes ozone (Crutzen, 1970). Ravishankara et al. (2009) noted that it is now the most important anthropogenic ozone-depleter. It is usually assumed that N_2O has no in situ atmospheric sources, although potential sources in the mesosphere-lower thermosphere (MLT) have been identified. One reaction mechanism postulated by Zipf and Prasad (1982), based on their laboratory work, is that secondary electron impact from energetic electron precipitation (EEP) promotes N_2 to the excited triplet state.

$$N_2\left(X^1\Sigma_g^+\right) + e^- \rightarrow N_2\left(A^3\Sigma_u^+\right) + e^-, \quad \text{(R1)}$$

where the $N_2(A^3\Sigma_u^+)$ state lies 7.63 eV above the $N_2(X^1\Sigma_g^+)$ ground state (Gillan et al., 1996). In a similar manner, reaction (R1) can be induced by photoelectrons (energetic electrons produced by photo-ionization of atmospheric species; Nagy & Banks, 1970). This is then followed by a reaction with O_2.

$$N_2(A^3\Sigma_u^+) + O_2 \rightarrow N_2O + O \quad \text{(R2a)}$$

to produce N_2O. The other, dominant (>70%) channel of $N_2(A^3\Sigma_u^+)$ + O_2 produces ground state N_2 and atomic oxygen.

$$N_2(A^3\Sigma_u^+) + O_2 \rightarrow N_2(X^1\Sigma_g^+) + 2O. \quad \text{(R2b)}$$

N_2O produced in the MLT would be transported down to the stratosphere through the winter polar vortex via seasonal mesospheric circulation (Fisher & O'Neill, 1993). Enhanced descent of such N_2O would be possible after a major sudden stratospheric warming (SSW) event, particularly if the stratopause reforms at significantly higher altitudes, as has occurred in several recent years (Manney et al., 2009).

Until recently, the mechanism suggested by Zipf and Prasad (1982) was largely disregarded as there were no high-altitude observations available to verify it. However, following measurements from the ACE-FTS (Atmospheric Chemistry Experiment-Fourier Transform Spectrometer) on-board SCISAT-1 and the MIPAS (Michelson Interferometer for Passive Atmospheric Sounding) instrument (Remedios et al., 2007) on-board Envisat, discussion of the potential for MLT production of N_2O was reopened. Using N_2O retrievals from ACE-FTS data limited to near 60 km, Semeniuk et al. (2008) argued that N_2O production in the upper mesosphere was highly likely. The authors suggested that it could be attributed to the reaction of ground state N with NO_2.

$$N(^4S) + NO_2 \rightarrow N_2O + O, \quad \text{(R3)}$$

peaking at around 75 km, where both reactants are produced via medium energy electron (MEE) impact in the mesosphere. Semeniuk et al. (2008) included reaction (R3) in the Canadian Middle Atmosphere Model (CMAM) and provided simulations that supported the satellite observations. Meanwhile, using MIPAS data limited to near 70 km, Funke et al. (2008) also suggested that the primary source of N_2O production in the MLT was likely to be reaction (R3). However, they acknowledged the potential for a significant contribution to enhancements from the lower thermosphere via the mechanism described by Zipf and Prasad (1982).

Sheese et al. (2016) provided first measurements of what appears to be this previously overlooked source, using v3.5 of the ACE-FTS data. Compared to the data available to Semeniuk et al. (2008), the altitude limit for N_2O was increased from 60 to 94.5 km by employing less conservative microwindow sets. These data were the first of its kind to extend into the lower thermosphere, up to where the signal is close to the noise (Boone et al., 2013). Mean N_2O volume mixing ratios (vmrs) on the order of 20–40 ppbv were reported for the polar winters near 94.5 km, decreasing to 10–20 ppbv at low latitudes. Note that the large vmrs do in fact correspond to small N_2O concentrations of ~10^5 molecules/cm^3 compared to typical near-surface N_2O concentrations of ~10^{13} molecules/cm^3. So far, there have been no corroborating observations to confirm this discovery, and to our knowledge, reaction (R2a) has not been included in any chemistry-climate model. In this study, we describe the inclusion of this production mechanism in the National Center for Atmospheric Research (NCAR) Whole Atmosphere Community Climate Model (WACCM) and compare a range of simulations to the ACE-FTS observations.

2. Method

2.1. WACCM

Model simulations were performed using a specified dynamics version of WACCM (SD-WACCM; Garcia et al., 2007; Marsh et al., 2013), which is part of the Community Earth System Model (CESM) v1.1.1 (Hurrell et al., 2013). In this study, we adapted the configuration of WACCM described in Kinnison et al. (2007) by adding the $N_2(A^3\Sigma_u^+)$ tracer and its accompanying chemistry through reactions (R2a), (R2b), and four other dominant $N_2(A^3\Sigma_u^+)$ depletion routes:

$$N_2(A^3\Sigma_u^+) + O \rightarrow N_2(X^1\Sigma_g^+) + O, \quad \text{(R4)}$$

$$N_2(A^3\Sigma_u^+) + N_2(X^1\Sigma_g^+) \rightarrow 2N_2(X^1\Sigma_g^+), \quad \text{(R5)}$$

$$N_2(A^3\Sigma_u^+) + N(^4S) \rightarrow N_2(X^1\Sigma_g^+) + N(^2P), \quad \text{(R6)}$$

$$N_2(A^3\Sigma_u^+) \rightarrow N_2(X^1\Sigma_g^+) + h\nu, \quad \text{(R7)}$$

Table 1
Configurations for WACCM Simulations Used in This Study

Simulation/configuration	$N_2(A^3\Sigma_u^+)$ production via EEP	$N_2(A^3\Sigma_u^+)$ production via photoelectrons	$N_2(A^3\Sigma_u^+) + O_2 \rightarrow N_2O + O$	$N(^4S) + NO_2 \rightarrow N_2O + O$	GLOW coupled
Standard	On	On	On	On	Yes
Control_0	Off	Off	Off	Off	No
Control_1	On	On	On	Off	Yes
Control_2	Off	Off	Off	On	No
Sensitivity_E	On	Off	On	On	No
Sensitivity_P	Off	On	On	On	Yes

Note. Includes simulation with all N_2O production sources switched on (Standard), three control simulations, and two sensitivity runs. All six model simulations were for the whole of 2013.

with rate constants from Herron (1999) (reactions (R4)–(R6)) and Shemansky (1969) (reaction (R7)). Reaction (R3) was already included in the existing configuration. The model has a horizontal resolution of 1.9° (latitude) × 2.5° (longitude) and 88 levels with a model top of 5.96×10^{-6} hPa (approximately 140 km). Vertical resolution in the MLT is roughly 3.5 km (Feng et al., 2013). We set the Prandtl number (Pr) for the production of turbulence from breaking gravity waves equal to 2, as in Feng et al. (2017). We performed six separate WACCM simulations with various combinations of N_2O reactions and mechanisms included (see Table 1).

The production rate of $N_2(A^3\Sigma_u^+)$ from EEP is given by the ion-pair production rates from MEE (~30–300 keV), measured by the Polar Orbiting Environmental Satellites (POES) as specified in Orsolini et al. (2018), Newnham et al. (2018), and Lam et al. (2010); and from auroral electrons (~1–30 keV) estimated from the parameterization of Roble and Ridley (1987). The reliability of the MEE ionization rate profile calculations is discussed in the supporting information. Meteorological variables (wind speed, temperature, and surface fluxes) in each simulation were nudged from surface to 50 km to the NASA Modern-Era Retrospective Analysis for Research and Applications (MERRA) reanalysis data with a 30-min time-step, as described in Rienecker et al. (2011) and Garcia et al. (2017). Variables were output as monthly means for all of 2013, a solar maximum and a major SSW year. Auroral electrons precipitate almost continuously; however, MEE levels are more sporadic as they are associated with geomagnetic storms, which were more frequent in 2013 compared to 2014 (Newnham et al., 2018). Simulations were run for one year before results were taken to allow for model spin-up time. Control simulations 0, 1, and 2 were performed to compare the relative importance of reaction (R2a) against reaction (R3) on the overall N_2O budget in the MLT. Sensitivity simulations E and P compare the altitude and latitude-dependent contributions of EEP and photoelectrons.

2.2. NCAR Global Airglow

The NCAR Global Airglow (GLOW) model (Solomon, 2017) was used to provide the photoelectron-induced production rate of $N_2(A^3\Sigma_u^+)$ over 2013. The required input parameters for GLOW include the Ap index and F107 (solar flux at 10.7 cm), which were taken from the National Oceanic and Atmospheric Administration (NOAA) database. The resulting three-hourly GLOW model output for the $N_2(A^3\Sigma_u^+)$ production rate was then interpolated onto the WACCM model grids.

2.3. Efficiency of N_2O Production

Since this is the first atmospheric modeling study of this phenomenon, we developed a new method to parameterize the impact of reaction (R2a) on the N_2O budget in the MLT. The method assumes that in the MLT the rate of in situ N_2O production balances the local chemical loss since N_2O is short-lived (~10 days at 95 km; Brasseur & Solomon, 2005); that is, N_2O is in steady state on a timescale of days and its production rate P can be set equal to the product of its first-order loss rate L and the observed concentration $[N_2O]_{obs}$

$$\frac{d[N_2O]}{dt} = P - L \cdot [N_2O]_{obs} = 0, \quad (1)$$

where loss occurs through photolysis and reaction with $O(^1D)$. For production, we consider EEP over the polar caps and photoelectrons at all latitudes. Hence,

$$\left(P_{\text{photo}}\cdot\alpha\right)+\left(P_{\text{EEP}}\cdot\alpha\right)=\left(\left(k_0\cdot\left[\text{O}\left(^1\text{D}\right)\right]\right)+J_{\text{N}_2\text{O}}\right)\cdot\left[\text{N}_2\text{O}\right]_{\text{obs}}, \quad (2)$$

where P_{photo} is the production rate of $N_2(A^3\Sigma_u^+)$ via photoelectrons, α is the probability that $N_2(A^3\Sigma_u^+)$ reacts with O_2 and makes N_2O via reaction (R2a), P_{EEP} is the production rate of $N_2(A^3\Sigma_u^+)$ via EEP, k_0 is the rate constant for the reaction between N_2O and $O(^1D)$ (Burkholder et al., 2015), and J_{N_2O} is the photolysis rate of N_2O.

The GLOW model (Solomon, 2017) provides a direct estimate for P_{photo}. P_{EEP} is calculated from EEP ion-pair production rates (Lam et al., 2010; Newnham et al., 2018; Orsolini et al., 2018; Roble & Ridley, 1987), multiplied by an $N_2(A^3\Sigma_u^+)$ production efficiency factor β (treated here as independent of altitude in the MLT). That is,

$$P_{\text{EEP}}=\left(I_{\text{MEE}}+I_{\text{aur}}\right)\cdot\beta, \quad (3)$$

where I_{MEE} and I_{aur} are the ionization rates due to MEE and auroral electrons, respectively. Substituting this into equation (2) yields an expression for β

$$\beta=\frac{\left(\left(k_0\cdot\left[\text{O}\left(^1\text{D}\right)\right]\right)+J_{\text{N}_2\text{O}}\right)\cdot\left[\text{N}_2\text{O}\right]_{\text{obs}}-\left(P_{\text{photo}}\cdot\alpha\right)}{\left(I_{\text{MEE}}+I_{\text{aur}}\right)\cdot\alpha}. \quad (4)$$

The branching ratio contained inside α is uncertain, with literature estimates ranging from <0.2% (Fraser & Piper, 1989) to 30% (Prasad & Zipf, 2000). To determine an optimal value of this in WACCM-GLOW, we performed test WACCM simulations with only the photoelectron contribution to $N_2(A^3\Sigma_u^+)$ production. Comparison with the observed N_2O in the MLT at low latitudes, where there is no impact from EEP, showed that a branching ratio of 0.5% was consistent with observations around 94.5 km. This value is within the literature range quoted above and was treated as a constant given that it should be independent of pressure and probably has a weak temperature dependence since (R2a) and (R2b) are both fast reactions (Zipf & Prasad, 1982).

The efficiency factor β was estimated using the 100–130 km zonal mean of each variable over the polar regions, as the auroral electron regime is considerably more regular than the MEE regime (a fixed value extrapolation was applied to $[N_2O]_{obs}$ above the satellite retrieval limit). This gave a value of 0.5 (rounded to one decimal place). We show in the supporting information that this value is consistent with laboratory measurements of integrated cross section for the excitation of $N_2 \rightarrow N_2(A^3\Sigma_u^+)$ and the ionization of N_2 (Cartwright et al., 1977; Itikawa, 2006), convolved with auroral electron energy spectra from Banks et al. (1974).

3. Results

Figure 1 shows latitude-height plots of the mean N_2O vmr for 2013, comparing the v3.6 ACE-FTS observations with WACCM simulation Standard (containing all sources), and three selected control and sensitivity simulations: Control_0 (the baseline for other simulations), Sensitivity_E, and Sensitivity_P (see Table 1). Plots extend from the stratosphere around 30 km up to 140 km in the lower thermosphere, though the ACE-FTS data only extend up to the satellite retrieval limit around 94.5 km. The N_2O vmrs for the ACE-FTS plots were calculated using the 5° running mean for each altitude level, as described by Sheese et al. (2016). The white spots and vertical bands in Figures 1a and 1b indicate where reliable means could not be calculated due to there being no or only one valid occultation in that location and time interval.

Inspection of the satellite plots (Figures 1a and 1b) shows patchy regions of N_2O throughout the midlatitude and low-latitude mesosphere, which are not reproduced by WACCM. Instead, a smooth N_2O distribution is simulated across all latitudes over the whole year (Figures 1c and 1d). The patchiness can be attributed to sampling frequency, as there are typically over a factor of 10 fewer occultations at lower latitudes (as the majority of ACE-FTS measurements are made at high latitudes), combined with a weaker signal at high altitude (Boone et al., 2013). This is verified in the supporting information, where the multiyear N_2O vmr climatology for v3.6 of the ACE-FTS data is shown.

Comparing the Standard run (Figures 1c and 1d) to ACE-FTS (Figures 1a and 1b) demonstrates first that a similar magnitude of N_2O to that observed is simulated near 94.5 km for both seasons (of order 10 ppbv), which supports the assumptions made when parameterizing the production of $N_2(A^3\Sigma_u^+)$ from EEP and photoelectrons (section 2.3). Second, good similarity in the vertical, latitudinal, and seasonal profiles is generally seen between model and satellite. There are two focal points of high N_2O vmrs: the lower stratosphere especially at low latitudes and the winter poles of the lower thermosphere. Clearly, the

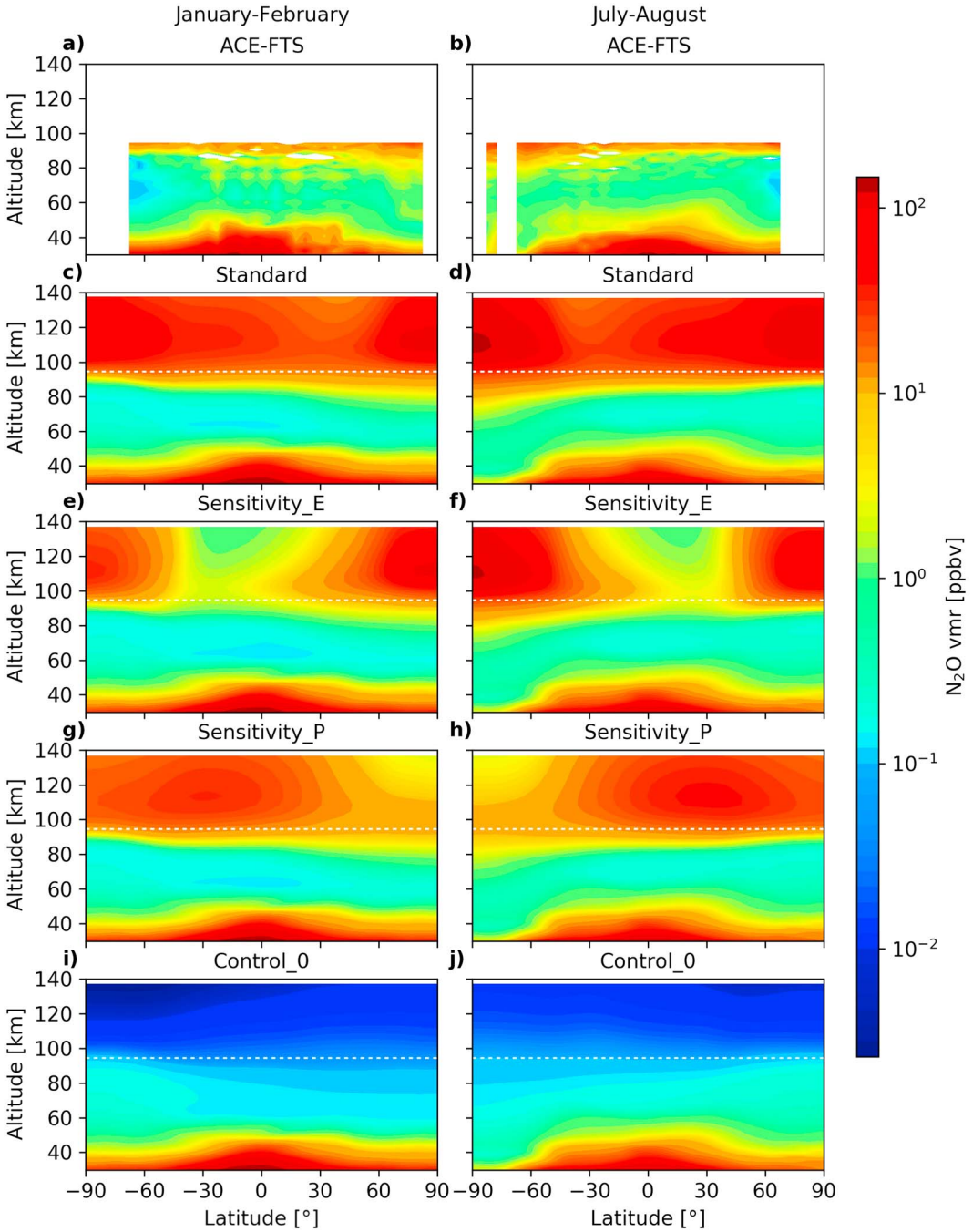

Figure 1. Latitude-height zonal mean cross sections of N_2O vmr (ppbv) averaged for (left column) January–February and (right column) July–August. Panels (a) and (b) show ACE-FTS satellite data for 2013, which extends up to 94.5 km. Panels (c)–(j) show four corresponding WACCM simulations (Table 1), where each *y* axis uses the simulated geopotential height for direct model comparisons. The horizontal dashed white line indicates 94.5 km.

majority of stratospheric enhancements can be attributed to surface sources distributed via the Brewer-Dobson circulation (Brewer, 1949; Dobson, 1956). In contrast, N_2O above the stratopause is produced in situ via reactions (R2a) and (R3). The seasonal changes of N_2O in the polar MLT can be explained by the efficiency of N_2O photolysis, the dominant route of removal. The model simulates larger vmrs (up to 40 ppbv) with a greater descent over the winter poles, as the lack of sunlight enables N_2O to persist during descent in the polar vortex. Conversely, lower values (around 10 ppbv) are found with much less

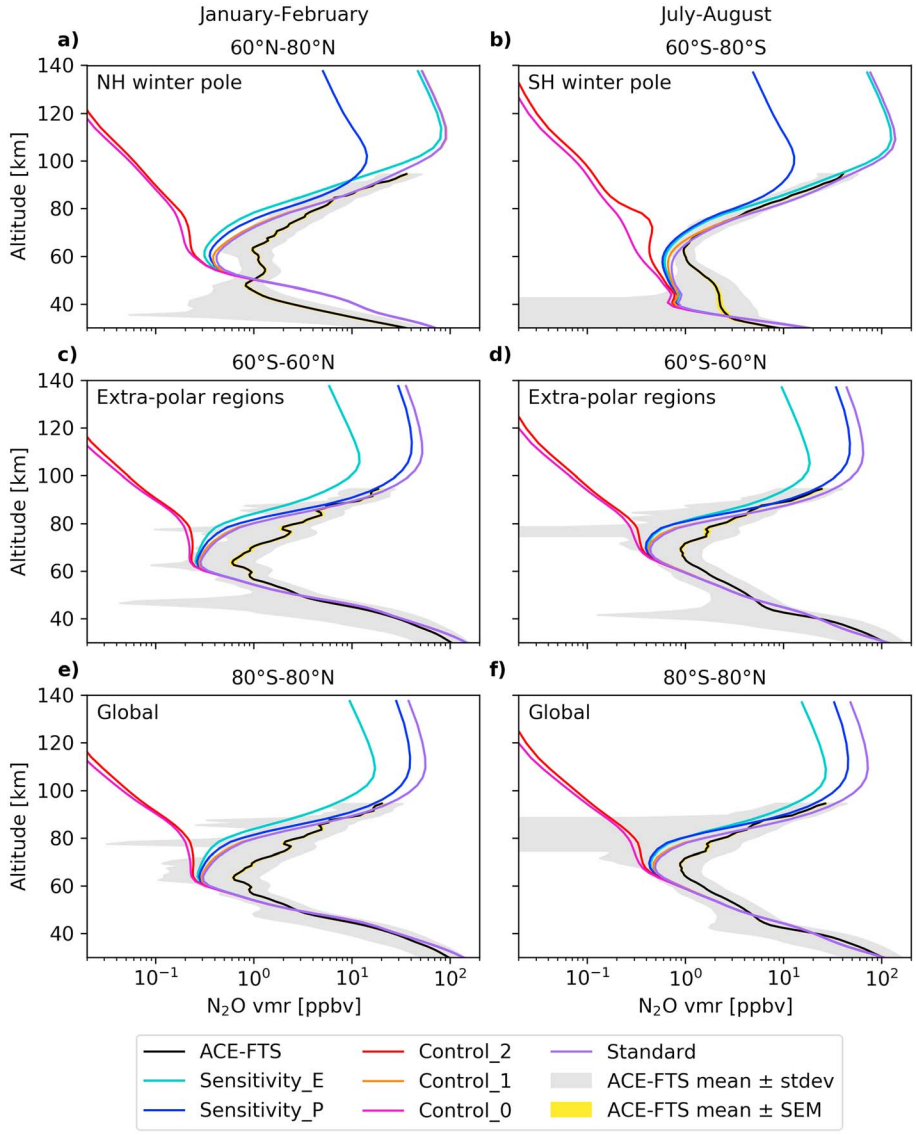

Figure 2. Altitude profiles of mean N_2O vmr (ppbv) from ACE-FTS observations compared with all six WACCM simulations (Table 1) averaged for (left column) January–February and (right column) July–August. The winter poles are shown in panels (a) and (b), the extra-polar regions in (c) and (d), and the global means in (e) and (f). The shaded regions indicate the ACE-FTS uncertainty with standard deviation (gray), and standard error of the mean (SEM) (yellow). Note that the average of the individual profile errors can be on the order of 50–200% in the MLT.

descent over the summer pole where N_2O is readily photolyzed. Further model-satellite agreement is seen over the extrapolar latitudes of the lower thermosphere, where simulations match the largely uniform N_2O vmrs of 10–20 ppbv. The only region showing obvious disagreement is the mesosphere between 60 and 80 km, particularly over midlatitudes and low latitudes, where less N_2O is simulated than observed.

For a more quantitative comparison of the features discussed above, we compare N_2O vmr profiles averaged over different latitude bands for two seasons (Figure 2). From about 80 km upward, simulation Standard follows the ACE-FTS profile closely for both seasons over all latitude bands. Given that the changes to the model primarily impact the MLT, this indicates that it now successfully captures the observed N_2O enhancements in this region. Interestingly, Control_1 is almost indistinguishable to Standard, meaning that in this altitude range, at least 99% of the N_2O production can be attributed to reaction (R2a). Reaction (R3) appears to be largely unimportant outside of mesospheric altitudes below 80 km. However, this mechanism is most prevalent in the Southern Hemisphere (SH) winter pole (Figure 2b). Here a maximum contribution of ~20% is seen

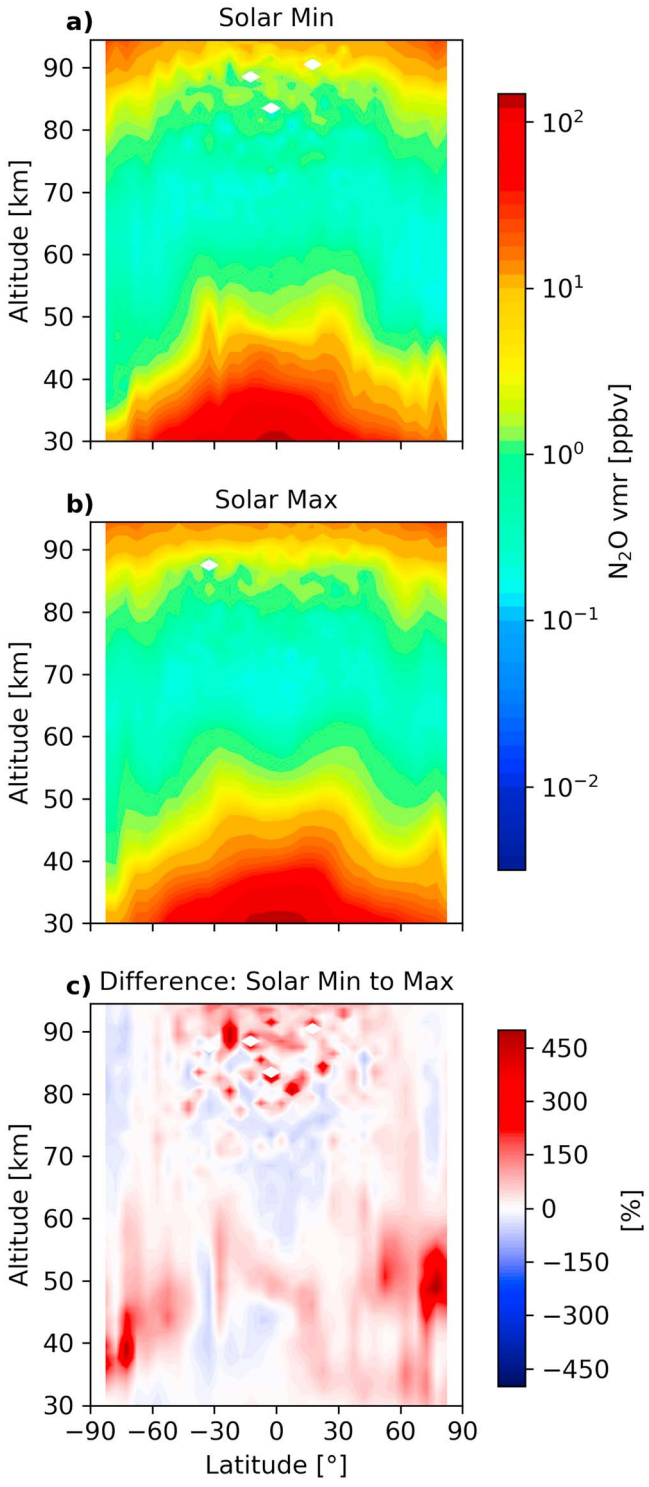

Figure 3. Solar cycle comparison: latitude-height zonal mean annual mean cross sections of ACE-FTS N_2O vmr (ppbv) for (a) 2008 near solar minimum and (b) 2014 near solar maximum. Panel (c) shows relative percentage difference at solar maximum with respect to solar minimum, where a +500% limit was applied to limit anomalies (characteristic of the calculation used on satellite data).

from Control_2 close to 60 km. Nevertheless, the remaining N_2O (~80%) is from reaction (R2a), yielding twice the upper limit suggested by Funke et al. (2008). From the similarity between 2013 and the N_2O vmr climatology in the supporting information, it is likely that these results would be closely replicated in simulations for different years.

Figures 2a and 2b highlight some apparent systematic differences between the model and satellite measurements. First, at around 60–80 km and 40–60 km for the north and south winter polar vortices, respectively, it appears that the model has a slower N_2O descent rate. This is most severe in the Northern Hemisphere where the N_2O vmr difference is up to a factor of 4, while it is only up to a factor of 2 in the SH. As this region appears challenging to simulate, it could be used as a future test for assessing model performance. Second, larger than measured (~5 times) N_2O vmrs are simulated below about 50 km in the Northern Hemisphere. If this is a model problem, it points to issues in the meridional stratospheric Brewer-Dobson circulation.

As expected from Figure 1, in Figures 2c–2f (which include the midlatitudes and low latitudes), simulation Standard typically underestimates the ACE-FTS N_2O by a factor of ~2 between 60 and 80 km. At this altitude, Semeniuk et al. (2008) suggest that the dominant N_2O production mechanism is reaction (R3). Therefore, a possible explanation for the shortfall could be that N_2O production via reaction (R3) is underestimated in the model because the simulated concentration of NO_2 (the source of N_2O in reaction (R3)) is too low. Unfortunately, v3.6 ACE-FTS retrievals of NO_2 do not extend into the mesosphere, so no direct comparison to our simulation can be made. A deficiency of NO_2 in the mesosphere could arise in WACCM either through underestimated vertical transport of NO_y from the thermosphere or the simplified ion chemistry in the ionospheric *D* region. This could be tested in future work using the very detailed *D* region ion chemistry recently included in versions of WACCM (Kovács et al., 2016). Longer simulations with such models could also provide quantification of the impact of upper atmospheric N_2O production on total stratospheric ozone destruction. Based on typical conversion efficiencies of N_2O to NO_y around an SSW event, Sheese et al. (2016) estimate the upper limit of this to be around 2%.

We compare the relative importance of contributions from EEP and photoelectrons to overall N_2O production via reaction (R2a) using the sensitivity simulations. In the polar regions, Figures 2a and 2b show that above ~90 km Sensitivity_E follows closely to Standard, whereas Sensitivity_P produces a vmr profile that is nearly a factor of 10 lower. This result indicates that almost all N_2O enhancements in the lower thermosphere during polar winter are caused by EEP, which is to be expected since there is very little sunlight to induce photoelectron production. However, there is significant MEE and auroral activity, resulting in large EEP rates. The conclusion that EEP is the principal driver of polar MLT N_2O can also be drawn by comparing Figure 1e (Figure 1f) and Figure 1g (Figure 1h). Figure 2c and 2d show that the situation in the extrapolar regions above about 90 km is the opposite. Here the majority of N_2O is produced via photoelectrons, as sunlight is present at midlatitudes and low latitudes throughout the year, but there is little incident EEP away from the polar caps (see again the relevant panels in Figure 1). The sensitivity simulations thus indicate the importance of including both EEP and photoelectrons in the model.

However, photoelectrons appear to be about twice as influential as EEP on the global N_2O budget in the lower thermosphere. This is evidenced most clearly by Figures 2e and 2f, which show the global mean altitude profiles; vmrs above 90 km from Sensitivity_P are roughly a factor of 2 larger than those from Sensitivity_E.

Figure 3 shows variations in the ACE-FTS data over the 11-year solar cycle. N_2O retrievals are plotted as annual means for 2008, near solar minimum (Figure 3a) and 2014, near solar maximum (Figure 3b). These years were selected to avoid the conflicting dynamical impact that would be found in major SSW years (e.g., 2009 and 2013). Figure 3c shows the magnitude of this variation as a percentage difference at solar maximum relative to solar minimum. Below 70 km, the deviations are most likely caused by varying N_2O transport by the Brewer-Dobson circulation over the solar cycle period, rather than the solar cycle itself. However, there is clearly more N_2O observed in the midlatitude and low-latitude MLT during solar maximum. Above 70 km there is a typical enhancement of ~10–100%, with values over 100% in some isolated areas. At solar maximum, solar irradiance intensity more than doubles at wavelengths required for photoionization ($<$100 nm; Brasseur & Solomon, 2005). Therefore, such increases could be anticipated from heightened photoelectron fluxes generating additional $N_2(A^3\Sigma_u^+)$ through reaction (R1). This supports the concept that photoelectrons have an important role in upper atmospheric N_2O production. In contrast, little difference is seen over the polar regions. A slightly negative deviation is even seen throughout the mesosphere, particularly in the SH. As recorded in the NOAA database, the increase in mean geomagnetic activity levels observed throughout 2014 compared to 2008 was relatively small (~25%). Since EEP is the dominant driver of $N_2(A^3\Sigma_u^+)$ production over the polar regions, the observed smaller solar cycle impact on N_2O concentration at high latitudes compared to midlatitudes and low latitudes is therefore expected. One reason for this is that solar minimum and maximum do not necessarily correspond to EEP minimum and maximum, which in this example both fell around a year later. Furthermore, the geomagnetic activity change during this solar cycle was small compared to the typical change (e.g., ~ +40% from 1996 to 2001 in the previous cycle).

4. Summary

The reaction between $N_2(A^3\Sigma_u^+)$ (produced via collisions between high energy electrons and N_2) and O_2 to form N_2O has been included for the first time in a chemistry-climate model. WACCM simulations provide strong quantitative support for the ACE-FTS observations of N_2O vmr enhancements above 90 km, first reported in Sheese et al. (2016). Essentially all of the N_2O enhancement ($>$99%) in the MLT occurs through the reaction of $N_2(A^3\Sigma_u^+)$ and O_2. Therefore, its inclusion in future modeling studies is essential for providing a description of N_2O production in the MLT. The reaction between N and NO_2 appears to be less important than previously suggested (Funke et al., 2008; Semeniuk et al., 2008), contributing no more than 20% of overall N_2O simulated at any altitude or latitude band in WACCM. However, this may in part be due to mesospheric NO_2 being underestimated in the model, something that could be investigated in a future study using a model with more detailed *D* region ion chemistry.

Latitudinal cross sections comparing the WACCM simulation against the ACE-FTS measurements generally show a good spatial agreement and replicate the seasonal N_2O variations observed near the poles. Both EEP and photoelectrons are found to play an important role in the production of $N_2(A^3\Sigma_u^+)$ and ultimately N_2O in the MLT. As expected, EEP is the dominant process near the poles, whereas photoelectrons are most significant in the extrapolar regions and contribute approximately twice as much as EEP to the global N_2O budget. Analysis of the ACE-FTS data over the extremes of the 11-year solar cycle show typical N_2O enhancements of ~10–100% during solar maximum, compared to solar minimum. Photoelectrons appear to be the more responsive process here, as the positive deviations are seen over the extrapolar latitudes of the MLT.

Acknowledgments
This project was funded by the Natural Environment Research Council (NERC) and the UK Met Office (NE/N008340/1). We acknowledge Stan Solomon who developed the GLOW model, Pekka Verronen who provided the MEE data, and Dan Marsh and David Jackson for helpful discussions. The WACCM simulations based on cesm1_1_1 were performed on the Polaris facility operated by the N8 HPC partnership. The source codes, input data for the WACCM simulations, and model output have been archived at the Leeds University PetaByte Environmental Tape Archive and Library (PETAL) and are available from C. W. K. or W. F. Source code for the GLOW model is available from https://www2.hao.ucar.edu, and data taken from the NOAA database are available from ftp://ftp.ngdc.noaa.gov/STP/GEOMAGNETIC_DATA/INDICES/KP_AP and ftp://ftp.swpc.noaa.gov/pub/weekly/RecentIndices.txt. The v3.6 ACE-FTS satellite data are available with registration from http://www.ace.uwaterloo.ca.

References

Banks, P. M., Chappell, C. R., & Nagy, A. F. (1974). A new model for the interaction of Auroral electrons with the atmosphere: Spectral degradation, backscatter, optical emission, and ionization. *Journal of Geophysical Research*, *79*(10), 1459–1470. https://doi.org/10.1029/JA079i010p01459

Boone, C. D., Walker, K. A., & Bernath, P. F. (2013). Version 3 retrievals for the Atmospheric Chemistry Experiment Fourier Transform Spectrometer (ACE-FTS). In P. F. Bernath (Ed.), *The Atmospheric Chemistry Experiment ACE at 10: A solar occultation anthology* (pp. 103–127). Hampton, VA: A. Deepak Publishing.

Brasseur, G., & Solomon, S. (2005). *Aeronomy of the middle atmosphere: Chemistry and physics of the stratosphere and mesosphere* (3rd ed.). Dordrecht, Netherlands: Springer. https://doi.org/10.1007/1-4020-3824-0

Brewer, A. W. (1949). Evidence for a world circulation provided by the measurements of helium and water vapour distribution in the stratosphere. *Quarterly Journal of the Royal Meteorological Society*, *75*(326), 351–363. https://doi.org/10.1002/qj.49707532603

Burkholder, J. B., Sander, S. P., Abbatt, J., Barker, J. R., Huie, R. E., Kolb, C. E., et al. (2015). Chemical kinetics and photochemical data for use in atmospheric studies, evaluation no. 18, JPL Publication 15–10. Pasadena, CA: Jet Propulsion Laboratory. Retrieved from http://jpldataeval.jpl.nasa.gov/

Cartwright, D. C., Trajmar, S., Chutjian, A., & Williams, W. (1977). Electron impact excitation of the electronic states of N_2. II. Integral cross sections at incident energies from 10 to 50 eV. *Physical Review A*, *16*(3), 1041–1051. https://doi.org/10.1103/PhysRevA.16.1041

Crutzen, P. J. (1970). The influence of nitrogen oxides on the atmospheric ozone content. *Quarterly Journal of the Royal Meteorological Society*, *96*(408), 320–325. https://doi.org/10.1002/qj.49709640815

Dobson, G. M. B. (1956). Origin and distribution of the polyatomic molecules in the atmosphere. *Proceedings of the Royal Society of London, Series A*, *236*(1205), 187–193. https://doi.org/10.1098/rspa.1956.0127

Feng, W., Kaifler, B., Marsh, D. R., Höffner, J., Hoppe, U.-P., Williams, P., & Plane, J. M. C. (2017). Impacts of a sudden stratospheric warming on the mesospheric metal layers. *Journal of Atmospheric and Solar - Terrestrial Physics*, *162*, 162–171. https://doi.org/10.1016/j.jastp.2017.02.004

Feng, W., Marsh, D. R., Chipperfield, M. P., Janches, D., Höffner, J., Yi, F., & Plane, J. M. C. (2013). A global atmospheric model of meteoric iron. *Journal of Geophysical Research: Atmospheres*, *118*, 9456–9474. https://doi.org/10.1002/jgrd.50708

Fisher, M., & O'Neill, A. (1993). Rapid descent of mesospheric air into the stratospheric polar vortex. *Geophysical Research Letters*, *20*(12), 1267–1270. https://doi.org/10.1029/93GL01104

Fraser, M. E., & Piper, L. G. (1989). Product branching ratios from the $N_2(A^3\Sigma_u^+)$ + O_2 interaction. *The Journal of Physical Chemistry*, *93*(3), 1107–1111. https://doi.org/10.1021/j100340a017

Funke, B., López-Puertas, M., García-Comas, M., Stiller, G. P., von Clarmann, T., & Glatthor, N. (2008). Mesospheric N_2O enhancements as observed by MIPAS on Envisat during the polar winters in 2002–2004. *Atmospheric Chemistry and Physics Discussions*, *8*(19), 5787–5800. https://doi.org/10.5194/acp-8-5787-2008

Garcia, R. R., Marsh, D. R., Kinnison, D. E., Boville, B. A., & Sassi, F. (2007). Simulation of secular trends in the middle atmosphere, 1950–2003. *Journal of Geophysical Research*, *112*, D09301. https://doi.org/10.1029/2006JD007485

Garcia, R. R., Smith, A. K., Kinnison, D. E., Cámara, Á. D. L., & Murphy, D. J. (2017). Modification of the gravity wave parameterization in the Whole Atmosphere Community Climate Model: Motivation and results. *Journal of the Atmospheric Sciences*, *74*(1), 275–291. https://doi.org/10.1175/jas-d-16-0104.1

Gillan, C. J., Tennyson, J., McLaughlin, B. M., & Burke, P. G. (1996). Low-energy electron impact excitation of the nitrogen molecule: Optically forbidden transitions. *Journal of Physics B: Atomic, Molecular and Optical Physics*, *29*(8), 1531–1547. https://doi.org/10.1088/0953-4075/29/8/017

Herron, J. T. (1999). Evaluated chemical kinetics data for reactions of $N(^2D)$, $N(^2P)$, and $N_2(A^3\Sigma_u^+)$ in the gas phase. *Journal of Physical and Chemical Reference Data*, *28*(5), 1453–1483. https://doi.org/10.1063/1.556043

Hurrell, J. W., Holland, M. M., Gent, P. R., Ghan, S., Kay, J. E., Kushner, P. J., et al. (2013). The Community Earth System Model: A framework for collaborative research. *Bulletin of the American Meteorological Society*, *94*(9), 1339–1360. https://doi.org/10.1175/bams-d-12-00121.1

Itikawa, Y. (2006). Cross sections for electron collisions with nitrogen molecules. *Journal of Physical and Chemical Reference Data*, *35*(1), 31–53. https://doi.org/10.1063/1.1937426

Kinnison, D. E., Brasseur, G. P., Walters, S., Garcia, R. R., Marsh, D. R., Sassi, F., et al. (2007). Sensitivity of chemical tracers to meteorological parameters in the MOZART-3 chemical transport model. *Journal of Geophysical Research*, *112*, D20302. https://doi.org/10.1029/2006JD007879

Kovács, T., Plane, J. M. C., Feng, W., Nagy, T., Chipperfield, M. P., Verronen, P. T., et al. (2016). D-region ion–neutral coupled chemistry (Sodankylä Ion Chemistry, SIC) within the Whole Atmosphere Community Climate Model (WACCM 4) – WACCM-SIC and WACCM-rSIC. *Geoscientific Model Development*, *9*(9), 3123–3136. https://doi.org/10.5194/gmd-9-3123-2016

Lam, M. M., Horne, R. B., Meredith, N. P., Glauert, S. A., Moffat-Griffin, T., & Green, J. C. (2010). Origin of energetic electron precipitation >30 keV into the atmosphere. *Journal of Geophysical Research*, *115*, A00F08. https://doi.org/10.1029/2009JA014619

Manney, G. L., Schwartz, M. J., Krüger, K., Santee, M. L., Pawson, S., Lee, J. N., et al. (2009). Aura Microwave Limb Sounder observations of dynamics and transport during the record-breaking 2009 Arctic stratospheric major warming. *Geophysical Research Letters*, *36*, L12815. https://doi.org/10.1029/2009GL038586

Marsh, D. R., Mills, M. J., Kinnison, D. E., Lamarque, J.-F., Calvo, N., & Polvani, L. M. (2013). Climate change from 1850 to 2005 simulated in CESM1(WACCM). *Journal of Climate*, *26*(19), 7372–7391. https://doi.org/10.1175/jcli-d-12-00558.1

Nagy, A. F., & Banks, P. M. (1970). Photoelectron fluxes in the ionosphere. *Journal of Geophysical Research*, *75*(31), 6260–6270. https://doi.org/10.1029/JA075i031p06260

Newnham, D. A., Clilverd, M. A., Rodger, C. J., Hendrickx, K., Megner, L., Kavanagh, A. J., et al. (2018). Observations and modelling of increased nitric oxide in the Antarctic polar middle atmosphere associated with geomagnetic storm driven energetic electron precipitation. *Journal of Geophysical Research: Space Physics*, *123*. https://doi.org/10.1029/2018JA025507

Orsolini, Y. J., Smith-Johnsen, C., Marsh, D. R., Stordal, F., Rodger, C. J., Verronen, P. T., & Clilverd, M. A. (2018). Mesospheric nitric acid enhancements during energetic electron precipitation events simulated by WACCM-D. *Journal of Geophysical Research: Atmospheres*, *123*, 6984–6998. https://doi.org/10.1029/2017JD028211

Prasad, S. S., & Zipf, E. C. (2000). Middle atmospheric sources of nitrous oxide (N_2O): O_2(B) and N_2(A) chemistry. *Physics and Chemistry of the Earth*, *25*(3), 213–222. https://doi.org/10.1016/S1464-1917(00)00008-8

Ravishankara, A. R., Daniel, J. S., & Portmann, R. W. (2009). Nitrous oxide (N_2O): The dominant ozone-depleting substance emitted in the 21st century. *Science*, *326*(5949), 123–125. https://doi.org/10.1126/science.1176985

Remedios, J. J., Leigh, R. J., Waterfall, A. M., Moore, D. P., Sembhi, H., Parkes, I., et al. (2007). MIPAS reference atmospheres and comparisons to V4.61/V4.62 MIPAS level 2 geophysical data sets. *Atmospheric Chemistry and Physics Discussions*, *7*(4), 9973–10017. https://doi.org/10.5194/acpd-7-9973-2007

Rienecker, M. M., Suarez, M. J., Gelaro, R., Todling, R., Bacmeister, J., Liu, E., et al. (2011). MERRA: NASA's Modern-Era Retrospective Analysis for Research and Applications. *Journal of Climate*, *24*(14), 3624–3648. https://doi.org/10.1175/jcli-d-11-00015.1

Roble, R. G., & Ridley, E. C. (1987). An auroral model for the NCAR thermospheric general circulation model (TGCM). *Annales de Geophysique*, *5A*(6), 369–382.

Semeniuk, K., McConnell, J. C., Jin, J. J., Jarosz, J. R., Boone, C. D., & Bernath, P. F. (2008). N_2O production by high energy auroral electron precipitation. *Journal of Geophysical Research*, *113*, D16302. https://doi.org/10.1029/2007JD009690

Sheese, P. E., Walker, K. A., Boone, C. D., Bernath, P. F., & Funke, B. (2016). Nitrous oxide in the atmosphere: First measurements of a lower thermospheric source. *Geophysical Research Letters*, *43*, 2866–2872. https://doi.org/10.1002/2015GL067353

Shemansky, D. E. (1969). N_2 Vegard–Kaplan system in absorption. *The Journal of Chemical Physics*, *51*(2), 689–700. https://doi.org/10.1063/1.1672058

Solomon, S. C. (2017). Global modeling of thermospheric airglow in the far ultraviolet. *Journal of Geophysical Research: Space Physics*, *122*, 7834–7848. https://doi.org/10.1002/2017JA024314

Zipf, E. C., & Prasad, S. S. (1982). A mesospheric source of nitrous oxide. *Nature*, *295*(5845), 133–135. https://doi.org/10.1038/295133a0